Journal of Materials Chemistry A

PAPER

View Article Online
View Journal | View Issue

Cite this: J. Mater. Chem. A, 2014, 2, 4055

A study of dye anchoring points in half-squarylium dyes for dye-sensitized solar cells†

Arthur Connell,[a] Peter J. Holliman,*[a] Matthew L. Davies,[a] Christopher D. Gwenin,[a] Sophie Weiss,[a] Mateusz B. Pitak,[b] Peter N. Horton,[b] Simon J. Coles[b] and Graeme Cooke[c]

This paper reports the synthesis of a series of new half-squaraine dyes (Hf-SQ) based around a common chromophoric unit consisting of linked indoline and squaric acid moieties. Carboxylate groups have been incorporated onto this core structure at four different points to study the influence of the anchoring group position on dye-sensitized solar cell (DSC) device performance. Dyes have been linked to TiO_2 directly through the squaric acid moiety, through a modified squaric acid unit where a vinyl dicyano group has replaced one carbonyl, *via* an alkyl carboxylate attached to the indole N or through a carboxylate attached to the 4 position of a benzyl indole. Contact angle measurements have been studied to investigate the hydrophobic/hydrophilic properties of the dyes and the results have been compared to N719 and Z907. Full characterization data of all the dyes and synthetic intermediates are reported including single-crystal X-ray structural analysis for dye precursors; the indole (**2a**) and the half-squarylium esters (**3a**) and (**6b**), as well as the dyes (**4c**), (**8**) and (**12**). Dye colours range from yellow to red/brown in solution (λ_{max} range from 430 to 476 nm) with ε ranging from 38 000 to 133 100 M^{-1} cm^{-1}. The performance of the dyes in DSCs shows the highest efficiency yet reported for a Hf-SQ dye (η = 5.0%) for 1 cm^2 devices with a spectral response ranging from 400 to 700 nm depending on the dye substituents. Co-sensitization of half-squarylium dye (**7b**) with squaraine dye (SQ2) resulted in a broader spectral response and an improved device efficiency (η = 6.1%). Density functional theory (DFT) calculations and cyclic voltammetry have been used to study the influence of linker position on dye HOMO–LUMO levels and the data has been correlated with *I–V* and EQE data.

Received 18th December 2013
Accepted 28th January 2014

DOI: 10.1039/c3ta15278b

www.rsc.org/MaterialsA

O'Regan and Grätzel's breakthrough in DSC devices used Ru bipyridyl dye N3 to sensitize nanoparticulate TiO_2.[1] Since 1991, Ru-bipy dyes have remained a widely used family of DSC dyes.[2] However, these dyes are expensive which is partly due to raw material costs but also due to lengthy purification procedures which hinder scaling and they have relatively low molar extinction coefficients (ε) and generally poor spectral response above 600 nm leading to DSC efficiencies of 11.1% for N719 (ref. 3) and 11.4% for C101.[4] This has led to the development of "Ru-free" organic DSC dyes (*e.g.* triphenylamines,[5] coumarins[6] and indolines[7]) which absorb in the same region as Ru-bipy dyes (450–600 nm) where AM1.5 solar intensity is highest. Generally, these organic dyes are simpler to purify than Ru-bipy complexes and have significantly higher ε. This allows thinner photo-electrodes to be used which can reduce recombination losses and improve device voltages. High ε is also advantageous when co-sensitizing the TiO_2 electrode to broaden spectral response because if fewer dye sorption sites utilized for the dye harvesting light at 400–650 nm, this leaves more space for near infrared (NIR) dyes which absorb at λ > 650 nm.

Extending DSC spectral response remains key to increasing device efficiency. This has led to the development of panchromatic dyes (*e.g.* "Black dye",[8] squaraine[9–12]). However, the synthetic and purification procedures associated with such dyes make them expensive and ensuring optimized spectral response across 400–900 nm in a single dye has proved very difficult. Co-sensitizing DSC photo-anodes with combinations of two or more dyes is another approach to increasing light harvesting[13–16] which has led to the first reports of ultra-fast co-sensitization[17,18] and η > 12% for a combination of porphyrin and triphenylamine dyes.[19]

Co-sensitization requires dyes which can harvest longer wavelength photons. In this context, squaraines have been studied as DSC dyes[20–22] because of their high ε and $\lambda_{max} \geq$ 650 nm where Ru-bipy dyes are less effective sensitizers.

[a]School of Chemistry, Bangor University, Gwynedd LL57 2UW, UK. E-mail: p.j.holliman@bangor.ac.uk; Fax: +44 (0)1248 370528; Tel: +44 (0)1248 382375

[b]UK National Crystallography Service, Chemistry, Faculty of Natural and Environmental Sciences, University of Southampton, Highfield Campus, Southampton, SO17 1BJ, UK

[c]WestCHEM, School of Chemistry, University of Glasgow, Glasgow, G12 8QQ, UK

† Electronic supplementary information (ESI) available. CCDC 977417–977428. For ESI and crystallographic data in CIF or other electronic format see DOI: 10.1039/c3ta15278b

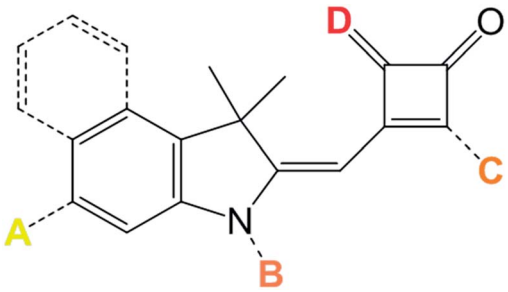

Scheme 1 Dye anchoring points on half-squaraine chromophore.

Half-squarylium (Hf-SQ) dyes are produced as an intermediate during the synthesis of unsymmetrical squaraine dyes.[23,24] Hf-SQ dyes are known to be fluorescent[25] and have been tested in ZnO giving $\eta = 0.27\%$ (ref. 26) 0.53%,[27] and, more recently, in TiO_2 DSC devices giving $\eta = 3.54\%$.[28] The Hf-SQ unit is also interesting because it offers a number of locations where a carboxylate anchoring group can be positioned. It is widely believed that the most efficient DSC dyes possess a donor–π bridge–acceptor (D–π–A) configuration.[29] In this paper, we have used the synthetic flexibility of the Hf-SQ moiety to investigate the influence of anchor position on DSC performance using a common chromophoric unit. Scheme 1 shows the anchor points tested (A/B = indole aromatic moiety, C = alkyl carboxylate on the indole N, D = carbonyl or vinyl dicyano moiety and E = H^+ for an acid or an alkyl group for an ester). We believe this the first report of this type. We have also investigated the effect of varying Hf-SQ side chain on dye/TiO_2 surface hydrophobicity. As such, this paper reports the synthesis of new Hf-SQ dyes along with detailed characterization, calculations of HOMO–LUMO energy levels and electron density distributions which have been correlated with DSC device testing. The co-sensitization of Hf-SQ and squaraine dyes has also been studied which offers the potential to reduce dye cost whilst also improving spectral response and device efficiency due to both sensitizers being prepared from the same synthetic pathway.

Results and discussion

Dye synthesis

The synthetic routes used to produce the Hf-SQ used in this work are shown in Schemes 1 and 2. The first step is the esterification of squaric acid in ethanol to give (**1**) which was prepared according to the method described by Terpetschnig *et al.* in good yield with spectroscopic data in line with the literature.[30] Compounds (**2a–c**) and (**5a–b**) were prepared using a general *N*-alkyl substitution reaction at the indole nitrogen with various iodo-alkanes.[31] All of the materials were prepared in high yield (>90%) with spectroscopic data in line with the literature.[31] The molecular structures of (**2a**), (**2b**) and (**5a**) have been confirmed by single crystal X-ray analysis (Fig. 1). Compounds (**2a–c**) and (**5**) were reacted with (**1**) to prepare (**3a–c**) and (**6**), respectively. In addition, single crystal analysis of (**3a**) shows the expected configuration (Fig. 1). Finally, hydrolysis of (**3a–c**) and (**6a–c**) using NaOH as described elsewhere[20,30] gives

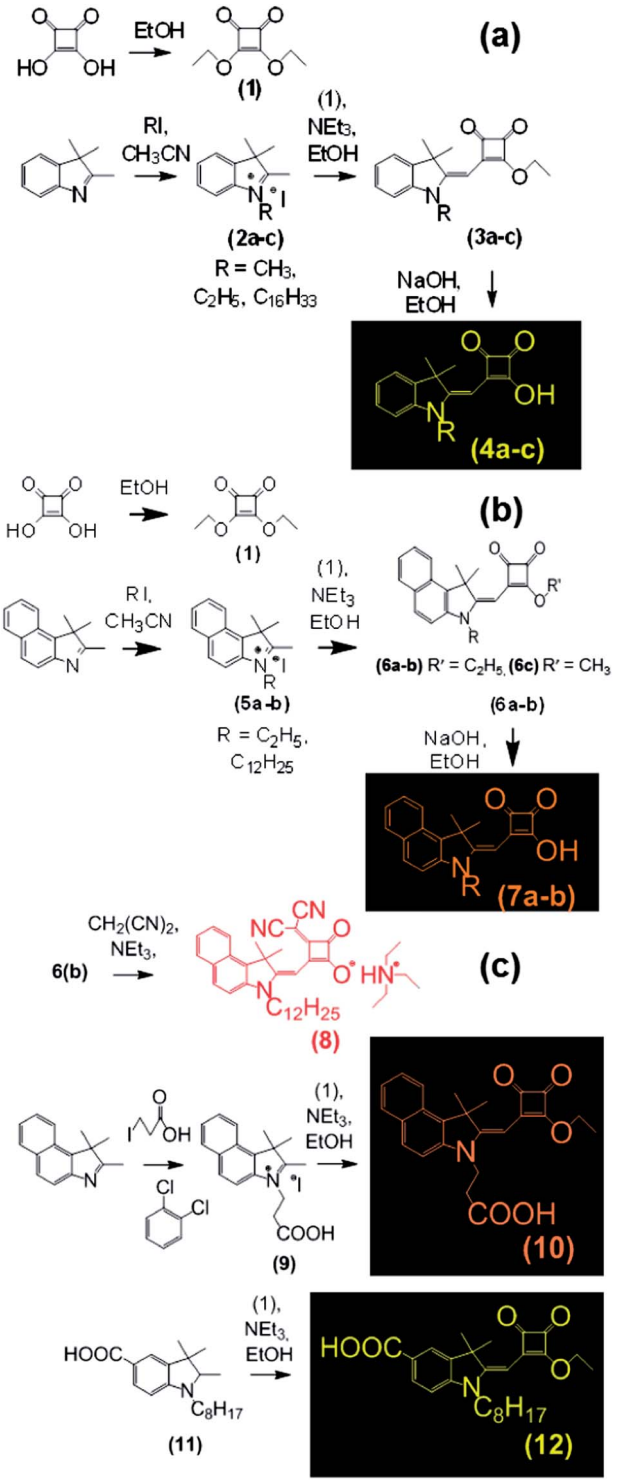

Scheme 2 Synthetic pathways to half-squaraine dyes.

the Hf-SQ dyes (**4a–c**) and (**7a–b**), respectively. The target compounds (**4a–c**) and (**7a–b**) were analyzed using ^1H and ^{13}C NMR, high resolution mass spectrometry, UV-visible spectroscopy, I.R. spectroscopy and melting points. In addition, single crystal analysis of (**4b**) and (**4c**) sodium salts show the expected molecular configuration as shown in (Fig. 3 and 4, ESI†). The synthetic routes to (**8**), (**10**) and (**12**) are shown in Scheme 2.

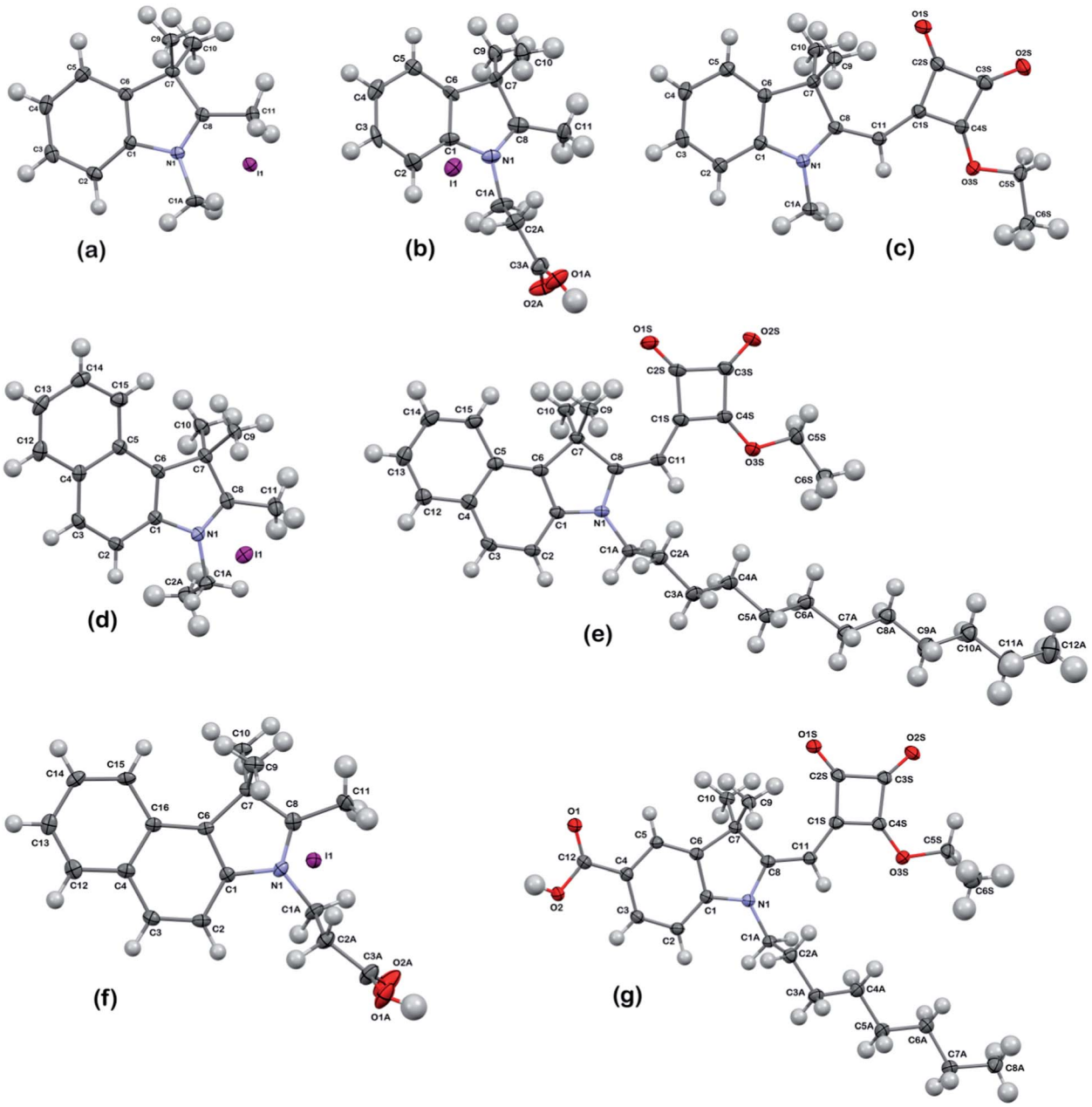

Fig. 1 Crystal structures of dye precursors and dyes (a) (**2a**), (b) (**2b**), (c) (**3a**), (d) (**5a**), (e) (**6b**), (f) (**9**) and (g) (**12**). Displacement ellipsoids – 50% probability.

In situ hydrolysis of (**6c**) together with nucleophilic substitution of a squaric acid carbonyl with malononitrile was used to prepare compound (**8**). These reaction conditions have been reported elsewhere in the literature for the preparation of related vinyl dicyano substituted Hf-SQ molecules.[23,32] Dye (**10**) and (**12**) were prepared by reacting (**9**)[33] and (**11**)[34] with (**1**), respectively. All of the dyes were isolated in high yield (>75%) and characterised using ^{1}H, ^{13}C NMR, high resolution mass spectrometry, melting points, infrared and UV-visible spectroscopy. The expected molecular configuration (**8**) (sodium salt) and (**12**) with the carboxylate linker groups sited on a vinyl dicyano-derivatized squaraine unit and on the benzyl of the indole, respectively have been confirmed by, single crystal X-ray analysis (Fig. 1) and (Fig. 6 ESI†). Whilst some structurally-related Hf-SQ dyes and their precursors have been reported previously,[20,30] (**5**), (**6b**), (**7b**) and (**8**) are variants (see ESI†) with a dodecyl chain attached to the nitrogen of the indole. The spectroscopic data for these new compounds are in line with the previously reported data (see ESI for references†). Dye (**10**) is significantly different to previously reported Hf-SQ dyes due to the linker being attached to the nitrogen of the indole. However, the ^{1}H and ^{13}C NMR of (**10**) show resonances in the expected regions for the various functional groups in the molecule and high resolution mass spectrometry has identified the expected

mass for this compound. In addition, the expected functional groups, including the carboxylate moiety, have been identified using infrared spectroscopy and (**10**) has a λ_{max} of 440 nm and an extinction coefficient of 116 000 M^{-1} cm^{-1} in ethanol measured using UV-visible spectroscopy.

The new dyes in this paper have been designed with bulky side groups to try to minimize inter-molecular interactions which can give rise to dye aggregation and increased recombination processes between adsorbed dye molecules on the TiO_2 surface. This is an established approach to DSC dye design, which has been described previously.[2,3] However, this can make it more difficult to grow single crystals for X-ray analysis which hinders structural studies of DSC dyes. Using careful purification and slow evaporation, it was possible to grow suitable crystals of several HF-SQ dyes and precursors reported including; (**4c**), the esterified precursor of (**7b**) *i.e.* (**6b**), (**8**) and (**12**). Analysis of the crystal structure obtained from (**4c**) *i.e.* the molecule containing the longest and potentially most hydrophobic alkyl unit (Fig. 4, ESI†) shows a complex structure where the negatively charged squaric acid moiety is balanced by sodium ions but with several molecules H-bonded together through the carbonyl and C–OH of this acyloin moiety (ESI, Fig. 5 and Table 4†). The hydrophobic hexadecyl alkyl chain is then arranged pointing away from the hydrophilic, electrostatically charged squaric acid linker group in the same way that might be observed in a surfactant. Interestingly, this localized arrangement is then extended to the wider crystal packing arrangement so that alternating layers of hydrophilic squaric acid and hydrophobic alkyl chains can be observed (Fig. 5, ESI†). This structural arrangement is important in the context of DSC devices because these dyes were designed with the hope that the charged, hydro-philic squaric acid moiety of the Hf-SQ dyes (**4a–c**), (**7a–b**) would chemisorb to the TiO_2 surface through a bi-dentate ester-like linkage whilst the long chain alkyl moiety might point away from the surface (Fig. 3). It was also hoped that this localized structure might extend to the inter-molecular packing arrangement of dyes on the TiO_2 surface creating a hydrophobic surface and that this might affect electrolyte–dye interactions and device stability in a similar manner to that which occurs for Z907 *versus* N719.[35] To test this hypothesis, contact angles have been measured for TiO_2 electrodes dyed either with N719, Z907, (**7b**), (**8**), (**10**) and (**12**) are shown in Fig. 2 and Table 1. The data show that films dyed with N719 have a lower contact angle and are relatively hydrophilic by comparison to films dyed with Z907 in line with literature reports[35,36] for these and other dyes incorporating various hydrophobic molecular entities such as the alkyl chains on Z907.[35] Interestingly, although (**7b**) and (**8**) both contain dodecyl alkyl chains attached to the nitrogen of the indole moiety, neither dye displays the expected hydrophobic properties that Z907 does with lower contact angles observed than for N719. Neither do (**7b**) or (**8**) show enhanced hydrophobicity relative to (**10**), which does not contain a long chain alkyl unit. By comparison, (**12**) does show a contact angle similar to Z907 despite possessing a shorter (octyl) alkyl chain compared to the longer, dodecyl unit in (**7b**) and (**8**). This suggests that hydrophobicity is also influenced by other factors as well as alkyl chain length. These are

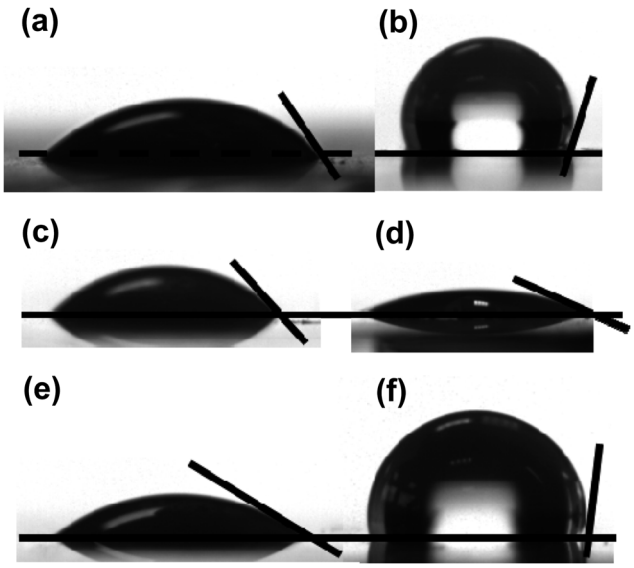

Fig. 2 Contact angle measurements and pictures for TiO_2 surfaces dyed with (a) N719, (b) Z907, (c) (**7b**), (d) (**8**), (e) (**10**) and (f) (**12**).

Table 1 Contact angles for dyes sorbed on TiO_2 photo-electrodes

Surface	Contact angle/°
N719	45.8 ± 3.0
Z907	110.1 ± 5.0
(**7b**)	42.3 ± 3.0
(**8**)	25.5 ± 3.0
(**10**)	38.7 ± 3.0
(**12**)	106.2 ± 4.0

believed to include the orientation of individual dye molecules on the surface which will, in turn, influence the orientation of the alkyl chain to the surface and, hence, any inter-molecular dye interactions and wider surface arrangement of dyes. All of these factors are important because contact angles only measure average surface hydrophobicity which results from the collective action of many molecules across the surface. For DSC dyes, such as Z907, where a dye monolayer is believed to form, it is reported that the alkyl chains are orientated towards the periphery of the adsorbed dye such that these groups will be the first part of the molecule in contact with any species approaching the TiO_2 surface. For the Hf-SQ dyes, the poor hydrophobicity of (**7b**) and (**8**) by comparison to (**10**) could be due to the alkyl chains being orientated in a way that does not point them towards the periphery of the molecule, or because a complete monolayer has not formed and/or because the alkyl chains do not form a collective surface. This is clearly not the case for (**12**) and therefore the position of the linker group and alkyl chains result in an orientation of the alkyl chain to repel hydrophilic species. Equilibrium dye loading measurements show that 81.7 μg cm^{-2} of (**7b**) sorbs to titania whilst (**10**) and (**12**) show comparable and much lower dye loadings at 33.9 and 34.0 μg cm^{-2}. It was not possible to measure the dye loading of (**8**) because this dye bleached rapidly and completely on

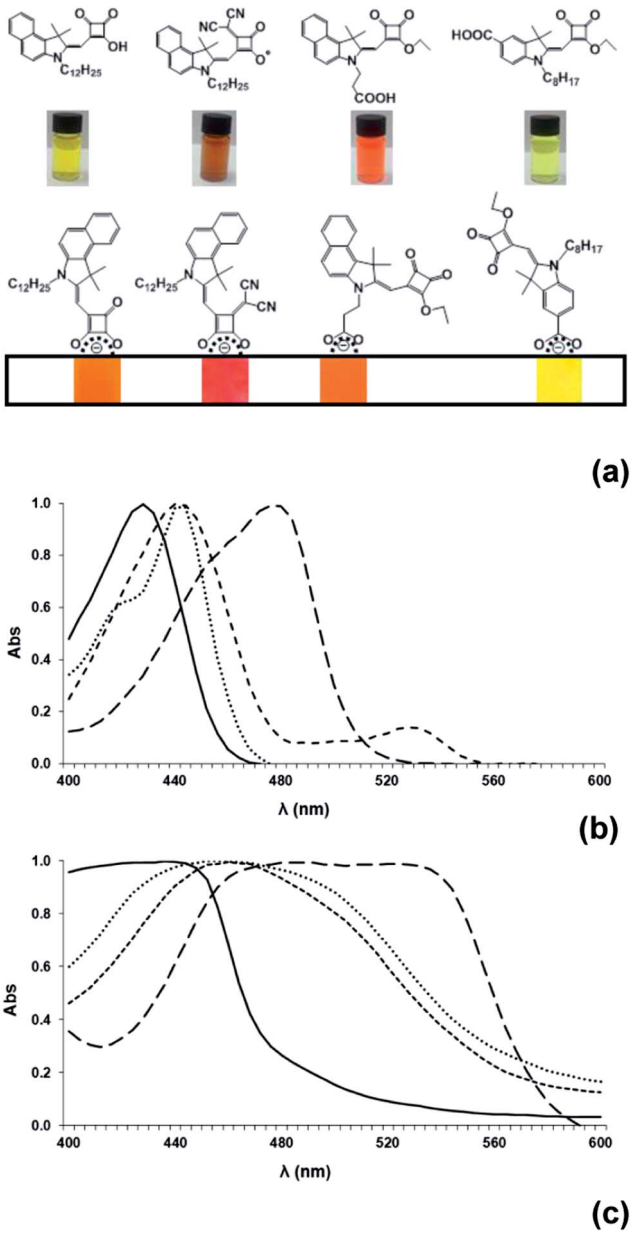

Fig. 3 (a) Colours and molecular configurations of selected dyes in solution and sorbed to TiO_2 and normalized UV-visible spectra of (b) dyes in solution and (c) dyes adsorbed onto TiO_2 films. Data show (**7b**) dotted line, (**8**) long dashes, (**10**) short dashes and (**12**) solid line.

exposure to alkali. Dye loading correlates with J_{sc} for (**7b**), (**10**) and (**12**) with the highest dye loading and J_{sc} for (**7b**) whilst lower dye loadings and J_{sc} are observed for (**10**) and (**12**). In addition, the broader spectral response of (**10**) relative to (**12**) explains the increased J_{sc} of (**10**) compared to (**12**). The dye loading data further suggest that dye orientation is important and appears to be more influential than dye loading when influencing contact angles (assuming dye uptake is complete). Interestingly, very low contact angles were observed for all dyes when measurements were made using the electrolyte solvent methoxypropionitrile instead of water suggesting complete wetting of the surface should occur in DSC devices. This should ensure the redox couple (I_3^-/I^-) is able to interact with the dye-oxide surface avoiding any dye regeneration limitations on device performance.

The optical properties of the dyes (**7b**), (**8**), (**10**) and (**12**) have been studied both in solution and adsorbed to translucent TiO_2 films (Fig. 3). (**12**) has a λ_{max} at 428 nm (133 100 M^{-1} cm^{-1}) in solution which red shifts to 444 nm when adsorbed to TiO_2. Bathochromic shifts are observed for (**7b**) (λ_{max} 442 nm, 38 000 M^{-1} cm^{-1}) and (**10**) (λ_{max} 440 nm, 116 000 M^{-1} cm^{-1}) in solution which are attributed to the increased conjugation from the naphthyl indole by comparison to the benzyl indole in (**12**). (**10**) also exhibits narrower absorption peaks than (**7b**) and the solution appears bright orange by comparison to the more diffuse yellow hue of (**7b**) and (**12**). Furthermore, a decrease in the extinction coefficient is observed for (**7b**) compared to (**6b**) which is similar to observations reported in the literature for other de-esterified Hf-SQ molecules.[26,28] A relatively large bathochromic shift and significantly broadened absorption peaks are observed for (**7b**) and (**10**) when adsorbed to TiO_2 (Fig. 3). To help understand these effects, the HOMO and LUMO maps for molecules (**7a**), (**8**), (**10**) and (**12**) have been calculated (Fig. 4). All of the dyes show that both the HOMO and LUMO are delocalized throughout the π-framework although there is significantly greater electron density for the LUMO around the squaric acid unit and at the nitrogen of the indole group. This should result in greater electronic interaction between the anchoring unit and TiO_2 surface which contributes to the broader absorption spectra for (**7a**), (**8**) and (**10**) which link *via* these groups by comparison to (**12**) which links *via* a benzyl carboxylate. Interestingly, the Hf-SQ–TiO_2 interface has also been investigated using DFT calculations by Cicero *et al.*[28] which also shows that the HOMO is delocalized through the π-framework of the whole structure while the LUMO contains a notable electron density contribution arising from the squaric acid group.[28] These workers reported that the HOMO–LUMO transition should therefore move electron density to the anchoring group resulting in directional electron transfer to the TiO_2 surface.[28] A similar phenomenon should also occur in the dyes reported here. Finally, incorporating the vinyl dicyano entity into the Hf-SQ central unit in (**8**) results in the largest peak broadening and bathochromic shift both in solution (λ_{max} 476 nm, 57 700 M^{-1} cm^{-1}) and when adsorbed to TiO_2 films. Whilst this influence of the electron donating vinyl dicyano group is similar to that reported for squaraines,[23,32] to the best of our knowledge, this effect has not yet been reported for half-squaraines.

DSC device testing

Table 2 shows *I–V* data for selected Hf-SQ devices. Initially, DSC devices were prepared with and without 5 mM the additive chenodeoxycholic acid (CDCA). However, the power conversion efficiencies of devices without CDCA were always at least 25% lower than those with CDCA; see *e.g.* (**10**) or (**12**) due to slight improvements in J_{sc}, V_{oc} and FF. This is in line with published reports that CDCA suppresses aggregation[28,32,37] and affects the position of the conduction band resulting in improved electron injection.[32,37]

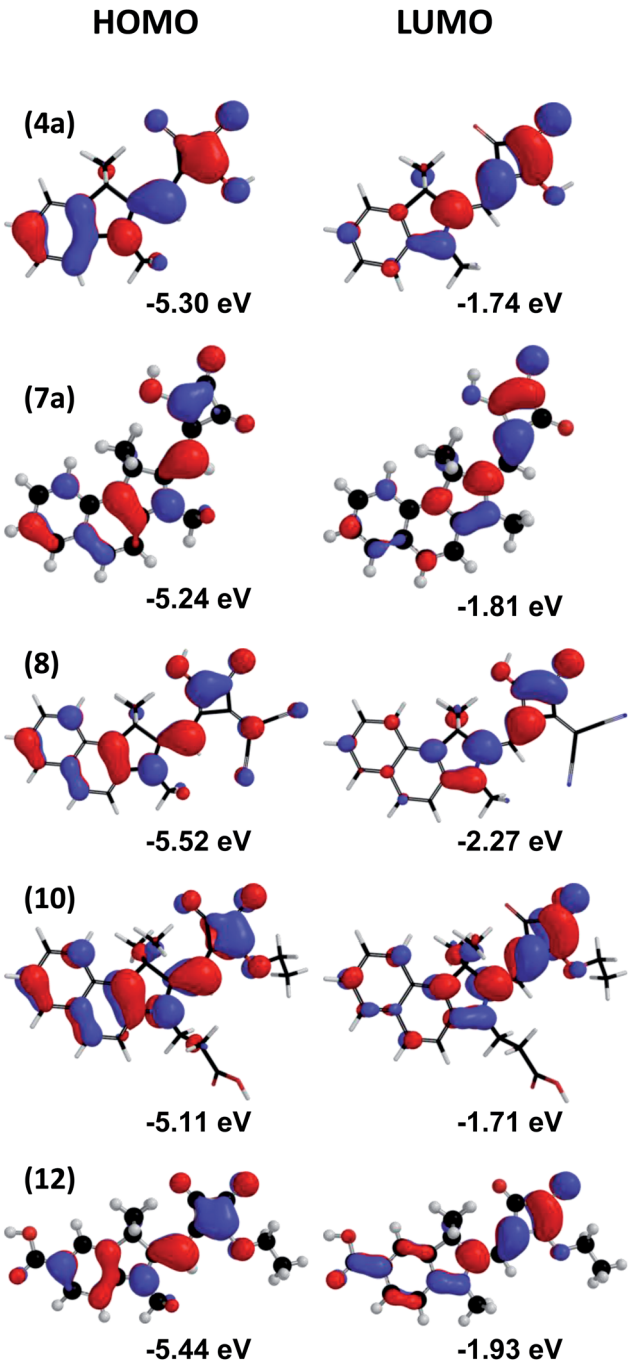

Fig. 4 Optimized geometries and HOMO and LUMO maps of the methyl indoline derivatives of selected dyes calculated using DFT.

Table 2 shows device data for TiO_2 devices sensitized with Hf-SQs containing either benzyl or napthyl indoles with alkyl chains of varying in length (ethyl to octadecyl). Comparing the benzyl indole dyes (**4a–c**) shows very similar device performance data for all three dyes with η ranging from 3.3–3.8%. The variance was mainly due to differences in J_{sc} which ranges from 7.9–9.2 mA cm^{-2} with very similar V_{oc} values observed for all three dyes (*ca.* 0.65 V). The slightly lower J_{sc} value was observed for the indole with the longest alkyl chain (hexadecyl) may reflect slightly poorer electron injection or dye regeneration from the electrolyte but this is only has a relatively small effect on η. However, after synthesis, this dye was also the most difficult to purify from the iodohexadecane precursor by comparison to the shorter chain iodoalkane dyes and precursors which may also have had a slight negative effect on J_{sc} for (**4c**).

Table 2 *I–V* data for DSC devices prepared using various half-squaraine dyes. Errors on device efficiencies are ±0.2%

Dye	η/%	FF	V_{oc}/V	J_{sc}/ mA cm^{-2}
Single dye devices				
(**4a**) + CDCA	3.3	0.56	0.64	9.20
(**4b**) + CDCA	3.8	0.62	0.66	9.22
(**4c**) + CDCA	3.5	0.67	0.63	7.92
(**7a**) + CDCA	4.0	0.61	0.60	10.90
(**7b**)	4.5	0.66	0.65	10.40
(**7b**) + CDCA	5.0	0.68	0.71	10.25
(**8**)	2.8	0.47	0.53	11.11
(**10**)	3.5	0.65	0.67	8.12
(**10**) + CDCA	3.9	0.68	0.68	8.38
(**12**)	2.4	0.74	0.61	5.31
(**12**) + CDCA	2.7	0.72	0.68	5.44
N719 only	6.4	0.60	0.73	14.69
Co-sensitized devices				
SQ2 + CDCA	3.4	0.67	0.62	8.25
(7) + SQ2 + CDCA	6.1	0.66	0.63	14.61

Studying the effects of alkyl chain length on the naphthyl indoles of dyes (**7a**) and (**7b**) shows two main differences. Firstly, a significant uplift in η is observed for the napthyl indoles (4.0–5.0%) compared to their benzyl indoles which mainly results from increased J_{sc} (10.2–10.9 mA cm^{-2}). This J_{sc} increase is attributed to a slight broadening of the absorption spectra due to the extended conjugation of the napthyl indole. This is in line with literature data for squaraines which report improved η for the napthyl indole squaraine, SQ2 *versus* the benzyl indole, SQ1.[20,21] Interestingly, for the napthyl indoles, increasing the length of the alkyl chain attached to the indole N from an ethyl group in (**7a**) to a dodecyl chain in (**7b**) increases V_{oc} from 0.61 to 0.71 V respectively. This is the highest V_{oc} observed for the Hf-SQ dyes reported here which, along with an improved FF, gives the highest single dye efficiency ($\eta = 5.0\%$). In addition, the V_{oc} of 0.61 V observed for (**7a**) is close to the literature value of 0.64 V reported elsewhere for this dye.[28] We believe this to be the highest efficiency Hf-SQ reported to date. The improved V_{oc} and FF may be due to decreased dye aggregation on the TiO_2 photo-electrode which could be caused by the longer alkyl chain in (**7b**) sterically reducing inter-dye interactions. Due to the improved device performance of (**7b**) by comparison to (**4a–c**) or (**7a**), the dye (**7b**) was taken forward for further study using co-sensitization studies and for comparison with dyes (**8**), (**10**) and (**12**).

Cyclic voltammetry (CV) measurements of (**7b**), (**8**), (**10**) and (**12**) in solution (10 mM in degassed THF) have been carried out to compare dye oxidation and reduction processes with spectral and DSC device data along with theoretical DFT calculations to try to further examine any structure–activity relationships arising from changes to the dye linker position. The CV data for

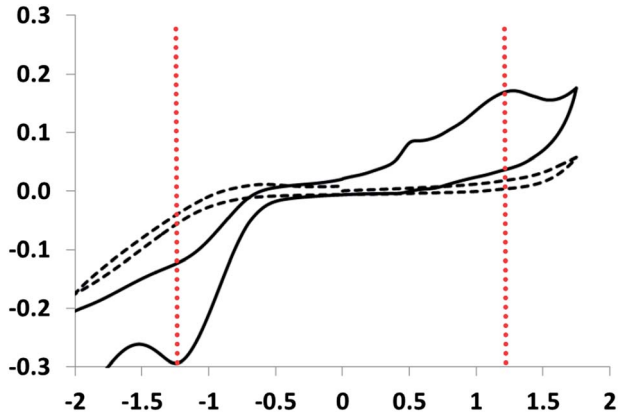

Fig. 5 Cyclic voltammetry data for 5 mM of (**8**) in degassed THF with $[Bu_4N]$ $[PF_6]$ as supporting electrolyte (solid line). Dashed line shows CV of supporting electrolyte only.

(**7b**) show three anodic waves (Fig. 5) similar to that reported in the literature.[27]

Shifts in the anodic and cathodic waves were observed for (**8**) and (**10**) which were expected from the changes in the electronic spectra of these dyes (Fig. 3). The CV data have been used to calculate the HOMO–LUMO potentials and band gaps *versus* the NHE and the band gap energies obtained correlate well with the onset of the absorption measured from the solution UV-Visible spectroscopy (Table 3). For example, the bandgap calculated from the absorption onset obtained for (**7b**), (**8**) and (**10**) is 2.20, 2.35 and 2.60 (eV) respectively which correlates with the bandgap energies of 2.23, 2.4 and 2.6 (eV) calculated from the CV data. By comparison, the anodic and cathodic waves measured for (**12**) are not as clear as for the other dyes (see ESI†). However, a sensible estimation of the HOMO–LUMO energy gap *i.e.* 2.62 (eV) could still be made by using the bandgap of 2.6 (eV) calculated from absorption onset obtained from solution UV-visible spectroscopy. Furthermore, both the DFT and CV data (Fig. 4 and 5) suggest that the LUMO levels of (**7b**), (**8**), (**10**) and (**12**) should be at the correct energy for successful electron injection from the dye into the TiO_2 conduction band and that the energy of the HOMO levels should enable successful regeneration of the dye using an I^-/I_3^- redox couple in the electrolyte.

To study the influence of linker position, the performance of (**7b**), (**8**), (**10**) and (**12**) were evaluated in DSC devices with and without CDCA (Table 2). Interestingly, it was not possible to include CDCA with (**8**) as this caused desorption of the sensitizer from the TiO_2 surface. However, where CDCA was present, device efficiency was consistently improved due to increased V_{oc} as has been widely reported in the literature for various dye systems.[38,39] Further desorption of (**8**) was also observed when an electrolyte was introduced into the device which meant that the *I–V* data for (**8**) was measured immediately after electrolyte addition. The desorption problems of (**8**) meant that, despite having the highest photocurrent of all dyes reported in this study ($J_{sc} > 11$ mA cm^{-2}), the overall efficiency was limited to $\eta = 2.8\%$ as a result of much lower V_{oc} and FF which must reflect the significant changes to the photo-electrode surface during desorption. These problems are ascribed to the addition of the vinyl dicyano group to one carbonyl of the squaric acid unit which in (**8**) must act as the linker group to the TiO_2 surface. This new group, rich in π-related electron density, presumably increases steric hindrance at the dye sorption site. Whilst this does not prevent the formation of an ester link between the dye and TiO_2 surface, it does appear to weaken this interaction to the extent that dye desorption occurs more easily. Indeed, desorption in the presence of the electrolyte suggests a dye binding energy of the same order as iodide which means the dye and electrolyte anions are competing for surface sorption sites. The instability of (**8**) is further evidenced by the fact that it bleaches on exposure to alkali (see earlier dye loading discussion).

Fig. 6 shows that the spectral responses of (**7b**), (**8**), (**10**) and (**12**) are all slightly red shifted by comparison to the corresponding absorption spectra of TiO_2 dyed films (Fig. 3). The

Table 3 Band-gap (E_B) calculated from the absorption onset, cyclic voltammetry and DFT calculations for dyes (**7b**), (**8**), (**10**) and (**12**)

Dye	λ onset/nm	E_B calc. from λ onset/eV	E_B calc. from CV/eV
(**7b**)	556	2.20	2.23
(**8**)	526	2.35	2.40
(**10**)	476	2.60	2.60
(**12**)	472	2.62	2.5

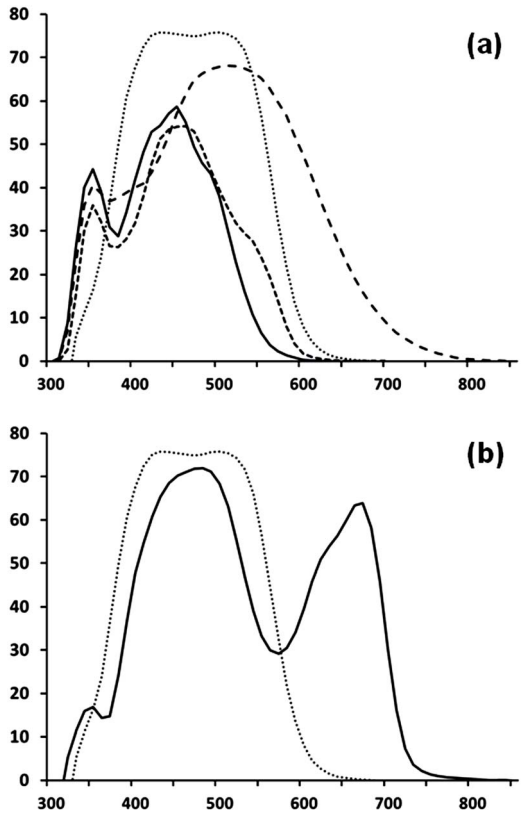

Fig. 6 EQE of (a) (**7b**) dotted line, (**8**) long dashes, (**10**) short dashes and (**12**) solid line and (b) (**7b**) dotted line and (**7b**) + SQ2.

narrowest spectral response and absorption data are observed for (**12**) which correlate with the lowest J_{sc} and η of these four dyes. Interestingly, the carboxylate linker in (**12**) is placed on the benzene ring and so is expected to lie furthest from greatest electron density of the LUMO on the squaraine moiety. In addition, (**12**) has the least conjugation of the 4 dyes tested here which limits the extent of spectral response. This is despite this dye having the highest ε of the four dyes tested here (133 100 M^{-1} cm^{-1}) which reflects the importance of electron injection over simply light harvesting. By comparison, the broadest spectral response (out to *ca.* 650 nm) and absorption data are observed for (**8**) which reflect the much greater conjugation in this molecule arising from the addition of the napthyl indole and vinyl dicyano moieties. The broader light harvesting gives rise to the highest J_{sc} despite this dye having a moderate ε of (57 700 M^{-1} cm^{-1}). Dye (**10**) shows a slightly broader spectral response compared to (**12**) at *ca.* 400 nm along with a shoulder at *ca.* 575 nm which is reflected in the higher J_{sc}; 8.12 *versus* 5.44 mA cm^{-2}. These two dyes have almost identically high ε relative to (**7b**) and (**8**) and although J_{sc} is improved for (**10**), it is lower than for (**7b**) which presumably is related the fact that the linker group is attached to the N of the indole. This means the linker is closer to the LUMO electron density on the squaraine ester but that electron injection must occur through the N of the indole. In squaraine dyes, it has been reported that charge generation occurs around the squaraine moiety during photo-excitation[40,41] but that electron transfer through the indole nitrogen such as that which occurs in the dye B1 is less efficient than through a pathway composed entirely of carbon and hydrogen atoms as occurs in SQ1.[20,33] The highest spectral response is observed for (**7b**) which approaches 75% between *ca.* 410 and 550 nm. This is despite (**7b**) having the lowest ε of these 4 dyes (38 000 M^{-1} cm^{-1}). This is ascribed to the linker group being the squaric acid moiety where DFT calculations (Fig. 4) show that the greatest LUMO electron density is found. Hence, electron injection should be enhanced by the proximity of the LUMO to the TiO_2 surface resulting in increased J_{sc} (over 10 mA cm^{-2}) despite significantly narrower spectral response than (**8**). To the best of our knowledge (**7b**) gives rise to the highest efficiency reported for a Hf-SQ DSC dye to date.

In an attempt to improve device and broaden the spectral response further towards the NIR, (**7b**) was co-sensitized with squaraine dye SQ2 using a fast pump dyeing method reported elsewhere.[17] The spectral response for a co-dyed (**7b**)/SQ2 device shows significantly greater light harvesting out to *ca.* 700 nm leading to a significant increase in J_{sc} to 14.61 mA cm^{-2} and η = 6.1% (Table 2). By comparison, an efficiency of 6.4% was obtained for a device sensitized using N719. In addition, the performance of this co-dyed device is very similar to many panchromatic SQ dyes reported[9–11] but has the advantage that a complicated synthesis is not required to incorporate the molecular entities required for higher energy photon harvesting across the solar spectrum. This could encourage research efforts to be directed towards incorporating molecular entities into dye systems that broaden the spectral response further into the near infrared as another approach alongside the development of panchromatic responses from individual dye systems.

Experimental

Instrumentation and chemicals

All chemicals were purchased from Aldrich and used as supplied unless otherwise stated. Anhydrous solvents were used as purchased except THF which was dried with Na wire. NMR spectra were recorded on a Bruker AC500 instrument operating at 500 MHz for ^{1}H and 125 MHz for ^{13}C. Chemical shifts (δ) are given in ppm relative to tetramethylsilane (for ^{1}H and ^{13}C). J values are given in Hz and refer to $J_{H,H}$ unless otherwise indicated. Mass spectra were recorded using electron impact, chemical ionisation (NH_3), fast atom bombardment, electrospray, matrix-assisted laser desorption ionisation and laser desorption ionisation at the EPSRC National Mass Spectrometry Service at the University of Swansea. Infrared spectra were recorded on a Perkin-Elmer 1600 series FTIR spectrometer. Elemental analysis was performed on a Carlo Erba EA1108 elemental analyser. Dye loadings were measured by desorption from 1 cm^2 TiO_2 electrodes using 40 mM Bu_4NOH in 1 : 1 v/v ethanol–water according the method described previously.[42] The concentration of dye in solution was measured using UV/Visible spectroscopy and dye loadings were calculated (μg cm^{-2}) using the appropriate ε (see ESI†) and the Beer–Lambert Law.

Cyclic voltammetry was measured on dyes (5 mM) at room temperature in N_2-saturated anhydrous tetrahydrofuran (THF) using 0.1 M tetrabutylammonium hexafluorophosphate (Bu_4NPF_6) as the supporting electrolyte. Measurements were performed using an Autolab PGSTAT 30 computer-controlled electrochemical measurement system (Eco Chemie, Holland). with a sweep rate of 0.05 V s^{-1} in a three-electrode cell with a glassy carbon (1 cm^2) working electrode, a silver/silver chloride (Ag/AgCl) reference electrode and a Pt sheet (1 cm^2) counter electrode. All voltammetric potentials were re-calculated and are reported *versus* NHE.

X-ray crystallography

Single-crystal X-ray diffraction analyses of **3a**, **4c_salt** and **5a** were performed at 120 K using a Bruker APEXII CCD diffractometer mounted at the window of a Bruker FR591 rotating anode (Mo Kα, λ = 0.71073 Å) and equipped with an Oxford Cryosystems Cryostream device. Data were processed using the COLLECT package.[43]

The X-ray data for compounds **2a**, **2b**, **4b_salt**, **6b**, **6c**, **9**, **12(I)** and **12(II)** were collected at 100 K on Rigaku AFC12 goniometer equipped with an enhanced sensitivity (HG) Saturn 724+ detector mounted at the window of an FR-E+ Superbright MoKα rotating anode generator with HF Varimax optics.[44]

The X-ray data for compound **8_salt** were collected with the use of synchrotron radiation at Diamond Light Source UK, beamline I19 (λ = 0.6889 Å) on a Crystal Logic diffractometer and Rigaku Saturn 724+ detector.

Unit cell parameters were refined against all data. For **3a**, **4c_salt**, **5a** an empirical absorption correction was carried out using SADABS,[45] whereas for **2a**, **2b**, **4b_salt**, **6b**, **6c**, **9**, **12(I)** and **12(II)** CrystalClear[46] software was used.

All structures were solved by direct methods and refined on Fo^2 by full-matrix least-squares refinements using programs of the SHELX-97/SHELX-2013 software.[47] All non-hydrogen atoms were refined with anisotropic displacement parameters. All hydrogen atoms were added at calculated positions and refined using a riding model with isotropic displacement parameters based on the equivalent isotropic displacement parameter (U_{eq}) of the parent atom.

The crystal structure of **4c_salt** is non-merohedraly twinned (180° rotation around 001 reciprocal vector). EvalCCD[48] was used to integrate the domains and the structure was refined using the HKLF 5 instruction in Shelxl.[47] The refined percentage ratio of the twin domains was 25 : 75 (refined BASF = 0.25714).

The crystal data for **8_salt** is not of the highest quality, but is sufficient to prove structural connectivity.

The long aliphatic chains present in the crystal structures of **8_salt** and **12(II)** are disordered and modelled over two sites.

For disordered components vibrational restraints (SIMU/DELU), similar displacement restraints (EADP) and distance/angle restraints DFIX/DANG used to maintain sensible geometries and atomic displacement ellipsoids. Some atoms required ISOR restraint to approximate isotropic behaviour. Crystal structure of **4b_salt** exhibits positional disorder which has been modelled over two sites. Additionally, in **4b_salt** highly diffused solvent electron density has been removed with PLATON/SQUEEZE routine.[49]

2a: $a = 6.944(2)$ Å, $b = 11.434(4)$ Å, $c = 15.743(6)$ Å, $\alpha = \beta = \gamma = 90°$; $V = 1249.9(8)$ Å^3, orthorhombic, $P2_12_12_1$, $Z = 4$, $\rho_{calc} = 1.600$ Mg m^{-3}; $\mu = 2.527$ mm^{-1}; $T = 100$ K; $\theta_{max} = 27.48°$, 8462 measured reflections, 2810 unique reflections [$R_{int} = 0.0230$], 2696 with $F^2 > 2\sigma$, $R(F, F^2 > 2\sigma) = 0.0151$; $R_w(F^2$, all data) = 0.0385; $\Delta\rho_{min/max} = 0.370/-0.230$ e Å^{-3}; CCDC: 977417.

2b: $a = 7.4137(5)$ Å, $b = 13.6430(12)$ Å, $c = 29.756(3)$ Å, $\alpha = \beta = \gamma = 90°$; $V = 3009.7(5)$ Å^3, orthorhombic, *Pbca*, $Z = 8$, $\rho_{calc} = 1.585$ Mg m^{-3}; $\mu = 2.123$ mm^{-1}; $T = 100$ K; $\theta_{max} = 25.02°$, 12 057 measured reflections, 2644 unique reflections [$R_{int} = 0.1625$], 1333 with $F^2 > 2\sigma$, $R(F, F^2 > 2\sigma) = 0.0486$; $R_w(F^2$, all data) = 0.0690; $\Delta\rho_{min/max} = 0.974/-0.595$ e Å^{-3}; CCDC: 977418.

3a: $a = 7.2314(2)$ Å, $b = 9.4760(3)$ Å, $c = 11.6165(4)$ Å, $\alpha = 82.094(2)°$, $\beta = 82.082(2)°$, $\gamma = 78.631(2)°$; $V = 767.95(4)$ Å^3, triclinic, $P\bar{1}$, $Z = 2$, $\rho_{calc} = 1.286$ Mg m^{-3}; $\mu = 0.087$ mm^{-1}; $T = 120$ K; $\theta_{max} = 27.48°$, 13 277 measured reflections, 3509 unique reflections [$R_{int} = 0.0435$], 2951 with $F^2 > 2\sigma$, $R(F, F^2 > 2\sigma) = 0.0542$; $R_w(F^2$, all data) = 0.1243; $\Delta\rho_{min/max} = 0.261/-0.212$ e Å^{-3}; CCDC: 977419.

4b_salt: $a = 8.810(4)$ Å, $b = 12.003(5)$ Å, $c = 17.977(8)$ Å, $\alpha = 82.678(14)°$, $\beta = 86.660(17)°$, $\gamma = 74.635(14)°$; $V = 1817.5(14)$ Å^3, triclinic, $P\bar{1}$, $Z = 2$, $\rho_{calc} = 1.211$ Mg m^{-3}; $\mu = 0.108$ mm^{-1}; $T = 100$ K; $\theta_{max} = 25.06°$, 26 587 measured reflections, 6434 unique reflections [$R_{int} = 0.0518$], 4237 with $F^2 > 2\sigma$, $R(F, F^2 > 2\sigma) = 0.0751$; $R_w(F^2$, all data) = 0.2457; $\Delta\rho_{min/max} = 0.747/-0.525$ e Å^{-3}; CCDC: 977420.

4c_salt: $a = 8.6755(7)$ Å, $b = 10.3795(8)$ Å, $c = 35.240(3)$ Å, $\alpha = 92.172(2)°$, $\beta = 91.370(2)°$, $\gamma = 99.956(3)°$; $V = 3121.7(4)$ Å^3, triclinic, $P\bar{1}$, $Z = 2$, $\rho_{calc} = 1.155$ Mg m^{-3}; $\mu = 0.087$ mm^{-1}; $T = 120$ K; $\theta_{max} = 24.71°$, 10 081 measured reflections, 10 081 unique reflections [$R_{int} = 0.000$], 8831 with $F^2 > 2\sigma$, $R(F, F^2 > 2\sigma) = 0.0958$; $R_w(F^2$, all data) = 0.2473; $\Delta\rho_{min/max} = 0.926/-0.404$ e Å^{-3}; CCDC: 977421.

5a: $a = 15.3349(3)$ Å, $b = 7.5158(2)$ Å, $c = 13.7564(2)$ Å, $\alpha = 90°$, $\beta = 92.5450(10)°$, $\gamma = 90°$; $V = 1583.92(6)$ Å^3, monoclinic, $P2_1/c$, $Z = 4$, $\rho_{calc} = 1.532$ Mg m^{-3}; $\mu = 2.010$ mm^{-1}; $T = 120$ K; $\theta_{max} = 27.48°$, 14 035 measured reflections, 2792 unique reflections [$R_{int} = 0.0390$], 2592 with $F^2 > 2\sigma$, $R(F, F^2 > 2\sigma) = 0.0217$; $R_w(F^2$, all data) = 0.0528; $\Delta\rho_{min/max} = 0.366/-0.367$ e Å^{-3}; CCDC: 977422.

6b: $a = 19.2363(14)$ Å, $b = 10.2830(7)$ Å, $c = 29.048(2)$ Å, $\alpha = 90°$, $\beta = 92.704(2)°$, $\gamma = 90°$; $V = 5739.5(7)$ Å^3, monoclinic, $C2/c$, $Z = 8$, $\rho_{calc} = 1.161$ Mg m^{-3}; $\mu = 0.073$ mm^{-1}; $T = 100$ K; $\theta_{max} = 25.02°$, 15 920 measured reflections, 5046 unique reflections [$R_{int} = 0.0461$], 4129 with $F^2 > 2\sigma$, $R(F, F^2 > 2\sigma) = 0.0401$; $R_w(F^2$, all data) = 0.1077; $\Delta\rho_{min/max} = 0.194/-0.182$ e Å^{-3}; CCDC: 977423.

6c: $a = 9.802(13)$ Å, $b = 9.8259(10)$ Å, $c = 15.69(2)$ Å, $\alpha = 83.509(10)°$, $\beta = 89.40(9)°$, $\gamma = 66.40(6)°$; $V = 1375(3)$ Å^3, triclinic, $P\bar{1}$, $Z = 2$, $\rho_{calc} = 1.178$ Mg m^{-3}; $\mu = 0.074$ mm^{-1}; $T = 100$ K; $\theta_{max} = 25.03°$, 15 659 measured reflections, 4847 unique reflections [$R_{int} = 0.0554$], 3510 with $F^2 > 2\sigma$, $R(F, F^2 > 2\sigma) = 0.0848$; $R_w(F^2$, all data) = 0.2128; $\Delta\rho_{min/max} = 0.593/-0.330$ e Å^{-3}; CCDC: 977424.

8_salt: $a = 11.9454(11)$ Å, $b = 12.4652(11)$ Å, $c = 24.378(2)$ Å, $\alpha = 90.54(2)°$, $\beta = 101.50(2)°$, $\gamma = 118.10(3)°$; $V = 3115.3(5)$ Å^3, triclinic, $P\bar{1}$, $Z = 2$, $\rho_{calc} = 1.210$ Mg m^{-3}; $\mu = 0.084$ mm^{-1}; $T = 100$ K; $\theta_{max} = 24.21°$, 22 317 measured reflections, 10 395 unique reflections [$R_{int} = 0.2525$], 2921 with $F^2 > 2\sigma$, $R(F, F^2 > 2\sigma) = 0.1277$; $R_w(F^2$, all data) = 0.4276; $\Delta\rho_{min/max} = 0.459/-0.422$ e Å^{-3}; CCDC: 977425.

9: $a = 7.530(2)$ Å, $b = 13.635(3)$ Å, $c = 34.164(8)$ Å, $\alpha = \beta = \gamma = 90°$; $V = 3507.9(15)$ Å^3, orthorhombic, *Pbca*, $Z = 8$, $\rho_{calc} = 1.550$ Mg m^{-3}; $\mu = 1.832$ mm^{-1}; $T = 100$ K; $\theta_{max} = 27.48°$, 21 886 measured reflections, 3992 unique reflections [$R_{int} = 0.0666$], 3503 with $F^2 > 2\sigma$, $R(F, F^2 > 2\sigma) = 0.0595$; $R_w(F^2$, all data) = 0.0896; $\Delta\rho_{min/max} = 0.908/-0.631$ e Å^{-3}; CCDC: 977426.

12 (polymorph I): $a = 12.7035(9)$ Å, $b = 18.2291(13)$ Å, $c = 11.1693(8)$ Å, $\alpha = 90.0°$, $\beta = 111.529(2)°$, $\gamma = 90.0°$; $V = 2406.1(3)$ Å^3, monoclinic, $P2_1/c$, $Z = 4$, $\rho_{calc} = 1.213$ Mg m^{-3}; $\mu = 0.083$ mm^{-1}; $T = 100$ K; $\theta_{max} = 27.48°$, 30 172 measured reflections, 5504 unique reflections [$R_{int} = 0.0562$], 4195 with $F^2 > 2\sigma$, $R(F, F^2 > 2\sigma) = 0.0406$; $R_w(F^2$, all data) = 0.1137; $\Delta\rho_{min/max} = 0.305/-0.199$ e Å^{-3}; CCDC: 977427.

12 (polymorph II): $a = 10.8885(8)$ Å, $b = 17.3070(11)$ Å, $c = 27.892(2)$ Å, $\alpha = 78.372(3)°$, $\beta = 80.234(3)°$, $\gamma = 77.874(3)°$; $V = 4988.8(6)$ Å^3, triclinic, $P\bar{1}$, $Z = 2$, $\rho_{calc} = 1.178$ Mg m^{-3}; $\mu = 0.081$ mm 1; $T = 100$ K; $\theta_{max} = 25.028°$, 47 382 measured reflections, 17 294 unique reflections [$R_{int} = 0.0964$], 9296 with $F^2 > 2\sigma$, $R(F, F^2 > 2\sigma) = 0.1066$; R_w (F^2, all data) = 0.3071; min/max = 1.222/−0.468 e Å^{-3}; CCDC: 977428.

Theoretical calculations

All calculations were performed using Spartan '08.[50] Geometries were first optimized semi-empirically (AM1) and then re-optimized using DFT (B3LYP/6-31G*) level of theory. The optimized structures were shown to be local minima on their respective

potential energy surfaces, as none of the vibrational frequencies in the optimized geometries generated imaginary frequencies.

Preparation of 1,1,2-trimethyl-1-dodecyl-1*H*-benzo[*e*]indole (5b)

A mixture of 1,1,2-trimethyl-1*H*-benzo[*e*]indole (8 g, 38 mmol) and dodecyl iodide (25 g, 87 mmol) was heated under reflux overnight under nitrogen in anhydrous acetonitrile (80 ml). After cooling, the solvent was removed *in vacuo* and the product was re-crystallized from ethyl acetate to give a green solid. (Yield 17.3 g, 90%.)

^{1}H NMR (400 MHz, $CDCl_3$) δ: 0.86 (q, J = 6.7 Hz, 2H), 1.03–1.41 (m, 14H), 1.41–1.60 (m, 1H), 1.73–1.91 (m, 4H), 1.97 (dd, J = 15.2 Hz, 7.8, 1H), 3.13–3.22 (m, 2H), 4.77 (t, J = 7.7 Hz, 1H), 7.72 (ddd, J = 29.6 Hz, 17.8 Hz, 8.1 Hz, 2H), 7.99–8.15 (m, 2H). ^{13}C NMR (101 MHz, $CDCl_3$) δ 7.41, 14.10, 15.27, 16.90, 22.64, 22.66, 22.73, 26.80, 28.18, 28.52, 29.13, 29.27, 29.31, 29.39, 29.44, 29.53, 29.59, 30.48, 31.85, 31.88, 33.55, 50.37, 55.30, 55.95, 76.83, 77.15, 77.36, 77.46, 112.53, 119.75, 122.49, 122.89, 124.41, 126.33, 127.65, 127.84, 128.69, 130.06, 131.47, 133.69, 137.17, 138.21, 195.17. MS (FTMS+) M^+ calculated = 378, M^+ observed = 378. *m*/*z* accurate mass (FTMS+), M^+ calculated = 378.1355, M^+ observed = 378.1359.

Preparation of 3-ethoxy-4-[(1-dodecyl-1,3-dihydro-3,3-dimethyl-2*H*-benzo[*e*]indol-2-ylidene)methyl]-3-cyclobutene-1,2-dione (6b)

(Yield 3 g, 65%). ^{1}H NMR (400 MHz, $CDCl_3$) δ 0.89 (t, J = 6.8 Hz, 3H), 1.27 (s, 16H), 1.38–1.54 (m, 4H), 1.58 (t, J = 7.1 Hz, 3H), 1.96–1.60 (m, 9H), 3.95 (t, J = 7.5 Hz, 2H), 4.95 (q, J = 7.1 Hz, 2H), 5.48 (s, 1H), 7.20–7.31 (m, 1H), 7.39 (t, J = 7.4 Hz, 1H), 7.55 (t, J = 7.3 Hz, 1H), 7.87 (dd, J = 13.4 Hz, 8.5, 2H), 8.12 (d, J = 8.5 Hz, 1H), ^{13}C NMR (101 MHz, $CDCl_3$) δ 14.13, 16.01, 22.68, 26.71, 26.99, 28.05, 29.32, 29.47, 29.54, 29.61, 31.91, 43.12, 49.84, 69.86, 76.78, 77.10, 77.30, 77.42, 80.90, 109.80, 122.22, 123.77, 127.19, 128.59, 129.58, 129.74, 130.82, 132.51, 139.82, 170.33, 173.30, 187.09, 187.14, 192.71. MS (FTMS+) $[M + H]^+$ calculated = 488, $[M + H]^+$ observed = 488, *m*/*z* accurate mass (FTMS+), reference compound: NH_4OAc, $[M + H]^+$ calculated = 488.3159, $[M + H]^+$ observed = 488.3153. FT-IR (KBr) ν/cm^{-1} 2988 (w), 1736 (m), 1707 (s).

Preparation of 4-[(1-dodecyl-1,3-dihydro-3,3-dimethyl-2*H*-benzo[*e*]indol-2-ylidene)methyl]-3-cyclobutene-1,2-dione (7b)

(Yield 2.5 g, 70%). ^{1}H NMR (400 MHz, MeOD) δ 0.89 (t, J = 6.8 Hz, 4H), 0.99–1.52 (m, 57H), 1.42 (dq, J = 14.6 Hz, 7.3, 19H), 1.56–1.91 (m, 18H), 1.95 (d, J = 5.9 Hz, 10H), 3.24 (dd, J = 10.0 Hz, 7.1 Hz, 14H), 3.33 (dt, J = 3.2 Hz, 1.6, 2H), 3.94 (t, J = 7.3 Hz, 2H), 4.90 (s, 2H), 5.73 (s, 1H), 7.28 (dd, J = 7.9 Hz, 5.0 Hz, 2H), 7.47 (s, 1H), 7.76–7.89 (m, 2H), 8.12 (d, J = 8.5 Hz, 1H). ^{13}C NMR (101 MHz, MeOD) δ 12.58, 13.08, 19.31, 19.32, 19.34, 21.36, 22.32, 23.39, 26.34, 26.61, 27.93, 29.02, 29.17, 29.19, 29.26, 29.32, 31.66, 42.11, 46.98, 47.20, 47.41, 47.62, 47.84, 48.05, 48.26, 48.72, 48.75, 49.25, 58.08, 58.11, 58.14, 82.60, 109.52, 121.66, 122.32, 126.27, 128.93, 128.96, 129.39, 130.29, 130.73, 140.97, 164.76, 176.55, 179.71, 196.59, 203.63. MS (FTMS+) $[M + H]^+$ calculated = 474, $[M + H]^+$ observed = 474, *m*/*z* accurate mass (FTMS+), reference compound: NH_4OAc, $[M + H]^+$ calculated = 474.3003, $[M + H]^+$ observed = 474.2998. FT-IR (KBr) ν/cm^{-1} 3473–3010 (m), 2960 (m), 1740 (s), 1600 (s). UV-Visible λ_{max} 442 nm (38 000 M^{-1} cm^{-1}) in ethanol.

Preparation of triethylammonium-2-[(1-dodecyl-3,3-dimethyl-1,3-dihydro-2*H*-indol-2-ylidene)-3-(dicyanomethylidene)-4-oxocyclobut-1-en-1-olate (8)

Triethylamine (1 ml, 7.14 mmol) was added dropwise to a mixture of (**6b**) (2 g, 6.15 mmol) and malononitrile (440 mg, 6.66 mmol) in ethanol (35 ml) and stirred for 2 h at room temperature. The solvent was removed *in vacuo* and the product was obtained as an orange solid after purification by column chromatography (SiO_2) with chloroform and methanol as eluent. (Yield 4.15 g, 75%).

^{1}H NMR (400 MHz, $CDCl_3$) δ 0.89 (t, J = 6.8 Hz, 4H), 1.06–1.61 (m, 33H), 1.61–2.01 (m, 11H), 3.33 (q, J = 7.3 Hz, 7H), 3.94 (s, 2H), 6.21 (s, 1H), 7.22 (d, J = 8.7 Hz, 1H), 7.28 (s, 3H), 7.35 (d, J = 7.6 Hz, 1H), 7.51 (t, J = 7.6 Hz, 1H), 7.85 (dd, J = 19.3 Hz, 8.4, 2H), 8.12 (d, J = 8.5 Hz, 1H). ^{13}C NMR (101 MHz, $CDCl_3$) δ 8.91, 14.12, 15.83, 22.68, 26.80, 29.33, 29.51, 29.60, 31.90, 39.20, 46.83, 69.71, 76.72, 77.04, 77.24, 77.35, 116.92, 118.39, 172.74, 179.07, 181.96, 192.83. MS (FTMS+) M^+ calculated = 623, M^+ observed = 623. *m*/*z* accurate mass (FTMS+), M^+ calculated = 623.4320, M^+ observed = 623.4317. FT-IR (KBr) ν/cm^{-1} 3473–3010 (s), 2960 (s), 2230 (s), 2210 (s), 1740 (s), 1600 (s). UV-Visible λ_{max} 476 nm (57 700 M^{-1} cm^{-1}) in ethanol.

Preparation of 3-ethoxy-(2-carboxyethyl)-[1,1,2-trimethyl-1*H*-benzo[*e*]indolium iodide-2-ylidene)methyl]-3-cyclobutene-1,2-dione (10)

(3 g, 70%). ^{1}H NMR (400 MHz, THF) δ 1.42 (t, J = 7.3 Hz, 8H), 1.47–1.89 (m, 38H), 1.94 (s, 13H), 2.08 (s, 1H), 2.76 (t, J = 7.3 Hz, 5H), 3.16 (q, J = 7.3 Hz, 6H), 3.30 (s, 1H), 3.62 (s, 23H), 4.32 (t, J = 7.3 Hz, 5H), 4.90 (q, J = 7.1 Hz, 5H), 5.53 (s, 2H), 7.35 (t, J = 7.5 Hz, 3H), 7.46–7.58 (m, 5H), 7.89 (dd, J = 8.3 Hz, 5.7, 5H), 8.22 (d, J = 8.5 Hz, 2H). ^{13}C NMR (101 MHz, THF) δ 5.83, 13.37, 24.18, 28.53, 36.63, 43.61, 47.56, 67.60, 79.00, 108.23, 120.23, 121.28, 124.79, 126.79, 127.34, 127.59, 129.09, 129.82, 138.01, 166.88, 169.68, 171.21, 185.32, 186.53, 189.90. MS (FTMS+) $[M + H]^+$ calculated = 406, $[M + H]^+$ observed = 406, *m*/*z* accurate mass (FTMS+), reference compound: NH_4OAc, $[M + H]^+$ calculated = 406.1649, $[M + H]^+$ observed = 406.1647. FT-IR (KBr) ν/cm^{-1} 3543–3060 (s), 2978 (w), 1738 (s), 1707 (s). UV-Visible λ_{max} 440 nm (116 000 M^{-1} cm^{-1}) in ethanol.

Device manufacture and testing

Photo-electrodes (0.5 × 2 cm = 1.0 cm^{-2}) were prepared by doctor blading two layers of TiO_2 colloid (DSL18NRT, Dyesol) followed by one layer of scattering TiO_2 colloid (WER4-O, Dyesol) onto fluorine tin oxide-coated glass (TEC15, 15 Ω □$^{-1}$). Each TiO_2 layer was calcined at 723 K for 30 min, then immersed in $TiCl_4$: THF_2 in deionised water (50 mM) at 343 K for 30 min, rinsed with de-ionised water, air-dried for 10 min and re-sintered at 723 K for 30 min. Counter electrodes were

prepared by drilling two holes *ca.* 2 cm apart through TEC8™ glass (NSG), washing with ^{i}PrOH and drying in air before depositing Pt colloid (Pt-1, Dyesol) and sintering at 400 °C for 30 min. The two electrodes were sealed together using a Surlyn™ (DuPont) gasket at 120 °C. Contacts were applied onto both electrodes using conductive silver paint (Agar).

Current–voltage characteristics were measured using an ABET Solar Simmulator with Xe arc lamp and a Keithley 2400 at 100 mW cm^{-2} or 1 Sun between 0 and 1 V. Spectral response measurements were made on a QEX10 Quantum Efficiency Measurement System in DC mode at resolution of 10 nm. Lamps were calibrated to 1 Sun (100 mW cm^{-2}) using a certified (Oriel 91150V) monocrystalline silicon reference cell traceable to the National Renewable Energy Laboratory (NREL).

Conclusions

This study shows that the position of dye anchoring points in half-squarylium dyes influences hydrophobicity and contact angle of dyes sorbed to TiO_2 surfaces. These phenomena are ascribed to the orientation of both individual dyes on the surface and the way in which sorbed dyes interact with each other such that hydrophobic surfaces consist of dye monolayers with hydrophobic chains perpendicularly arranged to the surface. Cyclic voltammetry measurements suggest the LUMO levels of all the dyes tested should be correctly positioned to enable electron injection from the dye excited state. However, the position of the linker group on the chromophore does affect the dye performance in DSC devices where improved J_{sc} and V_{oc} are observed for dyes where DFT calculations suggest the LUMO is located near to the squaraine linker moiety. Finally, we believe this is the first report of the ultra-fast co-sensitization of a dye precursor (Hf-SQ) with the associated full dye (squaraine) which is important in the context of extending spectral response whilst minimizing dye costs. Thus, co-sensitizing with two dyes from the same synthetic pathway reduces synthetic costs and results in similar device performance to panchromatic squaraines reported in the literature, which require much more complex and expensive synthetic procedures.

Acknowledgements

We gratefully acknowledge ERDF-WAG LCRI funding for SPARC (AC), EPSRC/TSB funding for SPECIFIC (EP/I019278/1) for MLD and AC, and the EPSRC UK National Mass Spectrometry Facility at Swansea University. We thank EPSRC for funding the National Crystallography Service (Southampton and Newcastle), and Diamond Light Source for access to synchrotron facilities.

Notes and references

1 B. O'Regan and M. Grätzel, *Nature*, 1991, **353**, 737.
2 A. Hagfeldt, G. Boschloo, L. C. Sun, L. Kloo and H. Pettersson, *Chem. Rev.*, 2010, **110**, 6595.
3 M. K. Nazeeruddin, F. De Angelis, S. Fantacci, A. Selloni, G. Viscardi, P. Liska, S. Ito, B. Takeru and M. Grätzel, *J. Am. Chem. Soc.*, 2005, **127**, 16835.
4 Y. Cao, Y. Bai, Q. Yu, Y. Cheng, S. Liu, D. Shi, F. Gao and P. Wang, *J. Phys. Chem. C*, 2009, **113**, 6290.
5 H. Im, S. Kim, C. Park, S.-H. Jang, C.-J. Kim, K. Kim, N.-G. Park and C. Kim, *Chem. Commun.*, 2010, **46**, 1335.
6 K. Hara, Z. S. Wang, T. Sato, A. Furube, R. Katoh, H. Sugihara, Y. D. Oh, C. Kasada, A. Shinpo and S. Suga, *J. Phys. Chem. B*, 2005, **109**, 15476.
7 S. Ito, S. M. Zakeeruddin, R. Humphry-Baker, P. Liska, R. Charvet, P. Comte, M. K. Nazeeruddin, P. Pechy, M. Takata, H. Miura, S. Uchida and M. Grätzel, *Adv. Mater.*, 2006, **18**, 1202.
8 M. K. Nazeeruddin, P. Péchy and M. Grätzel, *Chem. Commun.*, 1997, 1705.
9 S. Pack, H. Choi, C. Kim, N. Cho, S. So, K. Song, M. K. Nazeeruddin and J. Ko, *Chem. Commun.*, 2011, **47**, 2874.
10 J. H. Delcamp, Y. Shi, J.-H. Yum, T. Sajoto, E. Dell'Orto, S. Barlow, M. K. Nazeeruddin, S. R. Marder and M. Grätzel, *Chem. – Eur. J.*, 2013, **19**, 1819.
11 Y. Shi, R. B. M. Hill, J.-H. Yum, A. Dualeh, S. Barlow, M. Grätzel, S. R. Marder and M. K. Nazeeruddin, *Angew. Chem.*, 2011, **123**, 6749.
12 T. Maeda, S. Arikawa, H. Nakao, S. Yagi and H. Nakazumi, *New J. Chem.*, 2013, **37**(71), 701–708.
13 M. Guo, P. Diao, Y.-J. Ren, F. Meng, H. Tian and S.-M. Cai, *Sol. Energy Mater. Sol. Cells*, 2005, **88**, 23.
14 Y. Chen, Z. Zeng, C. Li, W. Wang, X. Wang and B. Zhang, *New J. Chem.*, 2005, **29**, 773.
15 D. Kuang, P. Walter, F. Nüesch, S. Kim, J. Ko, P. Comte, S. M. Zakeeruddin, M. K. Nazeeruddin and M. Grätzel, *Langmuir*, 2007, **23**, 10906.
16 J.-J. Cid, J.-H. Yum, S.-R. Jang, M. K. Nazeeruddin, E. M. Nez-Ferrero, E. Palomares, J. Ko, M. Grätzel and T. Torres, *Angew. Chem., Int. Ed.*, 2007, **46**, 8358.
17 P. J. Holliman, M. L. Davies, A. Connell, B. Vaca Velasco and T. M. Watson, *Chem. Commun.*, 2010, 7256.
18 P. J. Holliman, M. Mohsen, A. Connell, M. L. Davies, K. Al-Salihi, M. B. Pitak, G. J. Tizzard, S. J. Coles, R. W. Harrington, W. Clegg, C. Serpa, O. H. Fontes, C. Charbonneau and M. J. Carnie, *J. Mater. Chem.*, 2012, **22**(26), 13318.
19 A. Yella, H.-W. Lee, H. N. Tsao, C. Yi, A. K. Chandiran, M. K. Nazeeruddin, E. W.-G. Diau, C.-Y. Yeh, S. M. Zakeeruddin and M. Grätzel, *Science*, 2011, **334**, 629.
20 J.-H. Yum, P. Walter, S. Huber, D. Rentsch, T. Geiger, F. Nüesch, F. De Angelis, M. Grätzel and M. K. Nazeeruddin, *J. Am. Chem. Soc.*, 2007, **129**, 10320.
21 T. Geiger, S. Kuster, J.-H. Yum, S.-J. Moon, M. K. Nazeeruddin, M. Grätzel and F. Nüesch, *Adv. Funct. Mater.*, 2009, **19**, 2720.
22 H. Choi, J.-J. Kim, K. Song, J. Ko, M. K. Nazeeruddin and M. Grätzel, *J. Mater. Chem.*, 2010, **20**, 3280.
23 A. L. Tatarets, I. A. Fedyunyaeva, E. Terpetschnig and L. D. Patsenker, *Dyes Pigm.*, 2005, **64**, 125.
24 L. Beverina and P. Salice, *Eur. J. Org. Chem.*, 2010, 1207.
25 M. Matsui, T. Shibata, M. Fukushima, Y. Kubota and K. Funabiki, *Tetrahedron*, 2012, **68**, 9936.

26 M. Matsui, H. Mase, J.-Y. Jin, K. Funabiki, T. Yoshida and H. Minoura, *Dyes Pigm.*, 2006, **70**, 48.
27 G. Cicero, G. Musso, A. Lambertini, B. Camino, S. Bianco, D. Pugilese, F. Risplendi, A. Sacco, N. Shahzad, A. M. Ferrari, B. Ballarin, C. Barolo, E. Tresso and G. Caputo, *Phys. Chem. Chem. Phys.*, 2013, **15**, 7198.
28 G. Cicero, G. Musso, A. Lambertini, B. Camino, S. Bianco, D. Pugilese, F. Risplendi, A. Sacco, N. Shahzad, A. M. Ferrari, B. Ballarin, C. Barolo, E. Tresso and G. Caputo, *Phys. Chem. Chem. Phys.*, 2013, **15**, 7198.
29 L. Alibabaei, J.-H. Kim, M. Wang, N. Pootrakulchote, J. Teuscher, D. Di Censo, R. Humphry-Baker, J.-E. Moser, Y.-J. Yu, K.-Y. Kay, S. M. Zakeeruddin and M. Grätzel, *Energy Environ. Sci.*, 2010, **3**(11), 1757.
30 E. Terpetschnig and J. R. Lakowicz, *Dyes Pigm.*, 1993, **21**(3), 227.
31 L. J. S. Brown and P. A. Siesel, *Tetrahedron*, 1989, **45**(15), 4845.
32 T. Maeda, S. Mineta, H. Fujiwara, H. Nakao, S. Yagi and H. Nakazumi, *J. Mater. Chem. A*, 2013, **1**, 1303.
33 A. Burke, L. Schmidt-Mende, S. Ito and M. Grätzel, *Chem. Commun.*, 2007, 234.
34 S. Kuster, F. Sauvage, Md. K. Nazeeruddin, M. Grätzel, F. A. Nüesch and T. Geiger, *Dyes Pigm.*, 2010, **87**, 30–38.
35 M. Wang, S.-J. Moon, D. Zhou, F. Le Formal, N.-L. Cevey-Ha, R. Humphry-Baker, C. Grätzel, P. Wang, S. M. Zakeeruddin and M. Grätzel, *Adv. Funct. Mater.*, 2010, **20**, 1821.
36 G. C. Vougioukalakis, T. Stergiopoulos, A. G. Kontos, E. K. Pefkianakis, K. Papadopoulos and P. Falaras, *Dalton Trans.*, 2013, **42**, 6582.
37 J.-H. Yum, S. J. Moon, R. Humphry-Baker, P. Walter, T. Geiger, F. Nüesch, M. Grätzel and M. D. K. Nazeeruddin, *Nanotechnology*, 2008, **19**, 424005.
38 L. Jing, W. WenJun, Y. JiaBao, T. Jin, L. YiTao and H. JianLi, *Sci. China: Chem.*, 2011, **54**, 699.
39 M. G. Iglesias, J. J. Cid, J.-H. Yum, A. Forneli, P. Vazquez, M. K. Nazeeruddin, E. Palomares, M. Grätzel and T. Torres, *Energy Environ. Sci.*, 2011, **4**, 189.
40 X. Wang, J. Xu, M. Li, D. Fang, B. Chen, L. Wang and W. Xu, *RSC Adv.*, 2013, **2**, 5227.
41 A. L. Puyad, G. K. Chaitanya, A. Thomas, M. Paramasivam and K. Bhanuprakash, *J. Phys. Org. Chem.*, 2013, **26**, 37.
42 P. J. Holliman, K. J. Al-Salihi, A. Connell, M. L. Davies, E. W. Jones and D. A. Worsley, *RSC Adv.*, 2014, **4**(5), 2515–2522.
43 R. Hooft, *Collect: Data Collection Software*, B. V. Nonius, Delft: Netherlands, 1998.
44 S. J. Coles and P. A. Gale, *Chem. Sci.*, 2012, **3**, 683–689.
45 G. M. Sheldrick, *SADABS, Version 2.10*, Bruker AXS Inc., Madison, Wisconsin, USA, 2003.
46 CrystalClear-SM Expert 3.1 b26 (Rigaku, 20112).
47 SHELXL97/SHELX2013, G. Sheldrick, *Acta Crystallogr., Sect. A: Found. Crystallogr.*, 2008, **64**, 112–122.
48 A. J. M. Duisenberg, L. M. J. Kroon-Batenburg and A. M. M. Schreurs, An intensity evaluation method: EVAL-14, *J. Appl. Crystallog*, 2003, **36**, 220–229.
49 PLATON/SQUEEZE; (*a*) A. L. Spek, *Acta Crystallogr., Sect. A: Found. Crystallogr.*, 1990, **46**, C34; (*b*) P. v. d. Sluis and A. L. Spek, *Acta Crystallogr., Sect. A: Found. Crystallogr.*, 1990, (46), 194–201.

